Journal of Soft Computing Exploration

Homepage: htttps://shmpublisher.com/index.php/joscex

p-ISSN: 2746-7686
e-ISSN: 2746-0991

.

# Mix histogram and gray level co-occurrence matrix to improve glaucoma prediction machine learning

**Jumanto[1], Faizal Widya Nugraha[2], Agus Harjoko[3], Much Aziz Muslim[1,4], Noralhuda N. Alabid[5]**

[1]Department of Computer Science, Universitas Negeri Semarang, Indonesia
[2]Department of Computer, Politeknik Lamandau, Indonesia
[3]Department of Computer Science and Electronics, Universitas Gadjah Mada, Indonesia
[4]Department of Technology Management, Universiti Tun Hussein Onn Malaysia, Malaysia
[5]Department of Computer Science, University of Kufa, Iraq

**Article Info**

***Article history:***

Received Nov 30, 2022
Revised Dec 2, 2022
Accepted Dec 11, 2022

***Keywords:***

Glaucoma Detection
Histogram
GLCM
Texture Feature
Multi layer perceptron

**ABSTRACT**

Glaucoma is an eye disease that is the second leading cause of blindness. Examination of glaucoma by an ophthalmologist is usually done by observing the retinal image directly. Observations from one doctor to another may differ, depending on their educational background, experience, and psychological condition. Therefore, a glaucoma detection system based on digital image processing is needed. The detection or classification of glaucoma with digital image processing is strongly influenced by the feature extraction method, feature selection, and the type of features used. Many researchers have carried out various kinds of feature extraction for glaucoma detection systems whose accuracy needs to be improved. In general, there are two groups of features, namely morphological features and non-morphological features (image-based features). In this study, it is proposed to detect glaucoma using texture features, namely the GLCM feature extraction method, histograms, and the combined GLCM-histogram extraction method. The GLCM method uses 5 features and the Histogram uses 6 features. To distinguish between glaucoma and non-glaucoma eyes, the multi-layer perceptron (MLP) artificial neural network model serves as a classifier. The data used in this study consisted of 136 fundus images (66 normal images and 70 images affected by glaucoma). The performance obtained with this approach is an accuracy of 93.4%, a sensitivity of 86.6%, and a specificity of 100%.



***Corresponding Author:***

Jumanto,
Department of Computer Science,
Universitas Negeri Semarang,
Kampus Sekaran, Gunungpati 50229, Semarang, Indonesia.
Email: jumanto@mail.unnes.ac.id

## 1. INTRODUCTION

Glaucoma is one of the eye diseases suffered by a human. This disease is the second highest cause of blindness after cataracts [1]. The cases of glaucoma are predicted to continue to increase every year. There will be approximately 79.6 million people who suffer from glaucoma in 2020, and China is number 1 on the list of countries that contributes to glaucoma, followed by India and Europe. Meanwhile, in Indonesia, there are around 0.4% and 1.6% of the total population are estimated to suffer from glaucoma.

Glaucoma examination requires a lot of time and special tools. It also requires an ophthalmologist. Some of the commonly used imaging tools include fundus cameras, Optical Coherence Tomography (OCT) [2]–[14], Heidelberg Retinal Tomography (HRT) [15]–[23] and Confocal Scanning Laser Ophthalmoscopy (CSLO) [24]–[32] However, fundus cameras are the tools that are most commonly to find in healthcare centers or facilities [33]–[40].

Glaucoma examination carried out by an ophthalmologist is usually performed by directly observing the retinal image from the fundus camera. The results of the evaluation from one ophthalmologist may differ from other ophthalmologists. It is due to the doctor's experience, educational background, and psychological condition of the ophthalmologist [41]. Therefore a glaucoma diagnosis system based on digital image processing is needed to overcome the subjectivity of the specialists.

Research on glaucoma detection using digital image processing has been carried out by many previous researchers. Glaucoma detection or classification is greatly influenced by the feature extraction method, feature selection, and what features are used. In general, there are two groups of features used for glaucoma detection, namely morphological features and non-morphological features (image-based features) [25].

Research on glaucoma detection with non-morphological features, namely texture features was performed [42]. In this study, the feature extraction method of the Gray Level Co-occurrence Matrix (GLCM) was used; the result obtained an accuracy of 84.3%. This result can be developed to improve system performance, such as by creating additional feature extraction methods.

The feature extraction method proposed in this study used non-morphological features, namely the combination of GLCM feature extraction and histogram feature extraction. The histogram is a first-order statistical feature such as mean, standard deviation, entropy, and variance. Meanwhile, GLCM is a texture-based feature extraction that can reduce the misclassification of glaucoma images [43].

A study related to glaucoma classification with non-morphological features was a study by Archarya et al [44]. The study used two feature extraction methods, namely Higher-order spectra (HOS) and GLCM. The amount of data used was 60 fundus images (30 glaucomas, and 30 non-glaucomas or normal images). In this research, four classifiers were compared, namely: support vector machine (SVM), sequential minimal optimization (SMO), Naïve Bayes, and random forest. The best results are obtained from the random-forest classifier with an accuracy of more than 91%.

Touahri, et al. [45] performed glaucoma classification based on texture based image. This study employed a two-stage image processing and ensemble learning method. First stage, multiple modalities are generated from images using Gabor filter-based texture image synthesis. The second stage, every single dataset constructed from the respective modality will be trained to a single CNN classifier. The accuracy in this study was 89.6%.

Another study related to the texture analysis of fundus images was conducted by Yadav et al. [46]. In the study, the classification of glaucoma was carried out using the GLCM feature extraction method. The features of the GLCM used include contrast, homogeneity, energy, correlation, entropy, and standard deviation. Furthermore, these features are analyzed by reducing the Principal Component Analysis (PCA) dimension. The classifier used in this study is the Adaptive Resonance Theory I (ART I) model of neural networks. The accuracy obtained is 90%.

Another study discussing the diagnosis of glaucoma with invariant Haralick texture features and pyramid histogram oriented gradient (PHOG) was performed by Kamesh Sonti, et al. [47]. In this study, The quasi-bi-variate variational mode decomposition (QB-VMD) technique is used to decompose the retinal fundus images. Then, The frequencies acquired from QB-VMD when applied to PHOG and invariant Haralick texture features. The classifier used in this study is a blend of exponential polynomial support vector machines (EP-SVM) and bagged ensemble method. The accuracy obtained is 90%.

Using the method of feature extraction and the method of OD segmentation in the glaucoma detection system will affect the system's accuracy. The proper mix of OD segmentation, feature extraction, and proper classifier approaches can enhance performance in terms of accuracy. This study therefore proposes a novel and straightforward feature extraction strategy for detecting glaucoma in retinal fundus images.

## 2. METHOD

### Design System

The design of the glaucoma detection system is shown in Figure 1. In this design, a detailed system flow is presented for each process in the system consisting of two modules called the training module and the testing module.

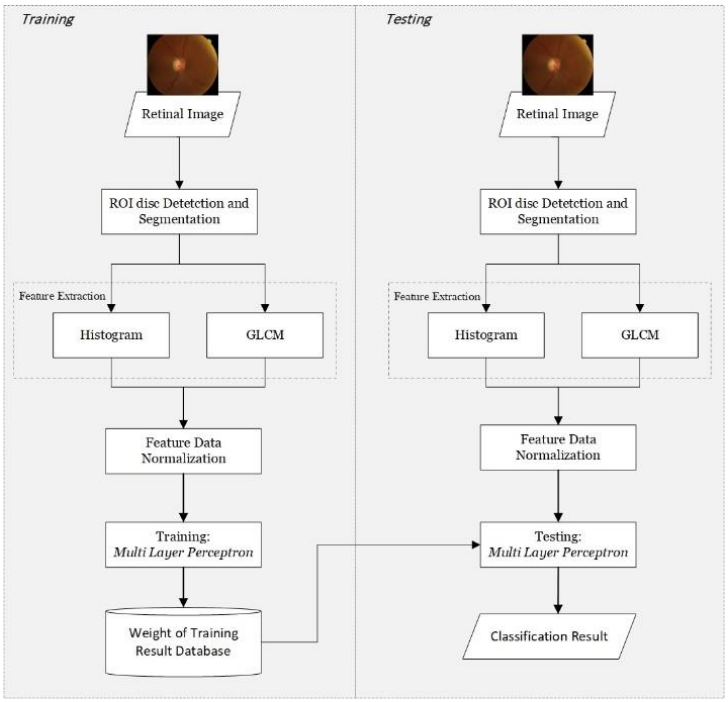


Figure. 1 Proposed method Block Diagram

Figure 1 shows the glaucoma detection system design consisting of two modules, the training module, and the testing module. The training module intends to obtain optimal MLP architecture. It can be achieved through several stages of the process starting from retinal image input, pre-processing (ROI detection and disc segmentation). Details of the ROI detection process can be seen in Fig. 3, and Fig 4 depicts disc segmentation process in detail. At the end of stage is feature extraction through feature normalization. The data resulting from feature normalization is then used as training data for MLP training.

The training process in the training module uses the backpropagation algorithm. It aims to produce optimal network architecture and weights. MLPs that have undergone the training process will then be used as classifiers in the testing module. The testing module is not much different from the process that occurs in the training module. However, after going through the feature normalization process, MLP will then recognize and classify it.

**Pre Processing**

1. Region of Interest (ROI) Disc Detection

ROI detection aims to localize the disc area of the input retinal image. The output of this process is a sub-image, which is then referred to as an ROI disc. The ROI detection carried out refers to research [4] whose process stages are shown in Figure 2.

The initial stage of the ROI disc detection process is thresholding on the green channel. It is performed because the center of the disc identification can be done easier in the green color channel [11]. The thresholding results still contain the non-disc area, especially on the edge of the retina. To remove the non-disc area, create a border mask. Making the border mask begins with local thresholding otsu on the red channel. A border mask is required for a reference pixel, which is the edge of the retina image, so edge operations are performed using the Sobel operator.

The next step is the process of dilating the image from the edge detection results. The result of the dilation operation is in the form of a mask that can remove noise at the edges of the retina. The final stage of disc ROI detection is to erase the non-disc area by applying equation (1).

$$Z = X - (X \cap Y) \tag{1}$$

Where X is image 2(c), Y is image 2(g).

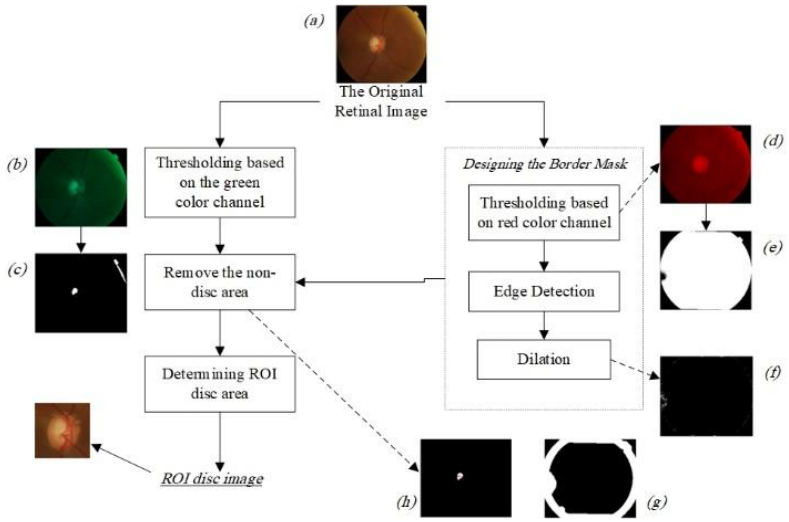


Figure. 2 ROI Detection Process [4]

2. Disc Segmentation

The disc segmentation process is carried out to produce a disc area separated from the area outside the disc. The image input in this process is the ROI disc image shown in Figure 2.

Figure 3 depicts the flow of the disc segmentation process. The initial stage of the disc segmentation process is the median filtering of the red color channel. It aims to remove noise, namely blood vessels. The next stage is thresholding with the otsu method to separate the object, in this case, the optical disc from the background. The results of the thresholding operation still contain a non-disc area so that it is subject to opening and dilation operations. The image of the opening and dilation operations becomes a reference for bounding boxes in the cropping process.

The next step is cropping the optical disc area 3 (f) to obtain the dominant disc image. After that, the median filtering operation will be used again to remove noise in the form of blood vessels. The next step is thresholding otsu to separate the optical disc area from the background. The results of the thresholding operation still contain the non-optical disc area. Therefore, opening and dilation operations will be performed on the result. The result of this process is then used as the reference for the segmentation of the optical disc area.

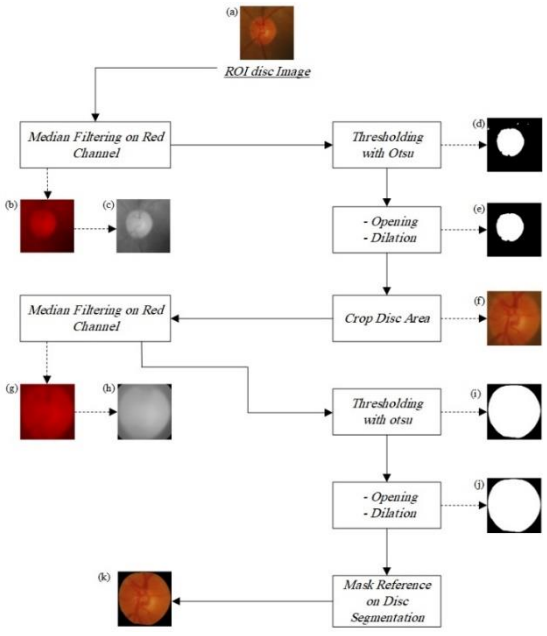


Figure 3 Disc Segmentation Processes

3. Feature Extraction

3.1 Histogram

A histogram is a statistical feature of the first order. In this study, there are six characteristics of the histogram features used, namely:

a. Mean

The components of the feature mean intensity *(mean)* is calculated based on equation (2).

$$mean = \sum_{i=0}^{L} i * p(i) \tag{2}$$

b. Standard Deviation

The calculation of Standard Deviation is shown in equation (3).

$$\sigma = \sqrt{\sum_{i=0}^{L} (i-m)^2 \, p(i)} \tag{3}$$

c. Skewness

The skewness feature is a measure of the asymmetry of the mean intensity. The calculation is shown in equation (4).

$$skewness = \sum_{i=0}^{L} (i-m)^3 \, p(i) \tag{4}$$

a. Energy

Energy is a measure that tells the distribution of pixel intensity over the range of the gray level. The calculation is shown in equation (5).

$$energi = \sum_{i=0}^{L} [p(i)]^2 \tag{5}$$

b. Entropy

Entropy indicates the complexity of an image. The entropy calculation is shown in equation (6).

$$entropi = -\sum_{i=0}^{L} p(i) \, log_2(p(i)) \tag{6}$$

c. Smoothness

The smoothness feature is included to measure the level of smoothness/roughness of the images' intensity. The smoothness calculation is shown in equation (7).

$$R = 1 - \frac{1}{1+\sigma^2} \tag{7}$$

3.2 Gray Level Co-occurrence Matrix (GLCM)

GLCM is a method to analyze the texture features of an image. Ordinary as a second-order statistical analysis. The GLCM calculates statistical features based on the degree of the grayness of an image. The GLCM method proposed by Harralick [12] contains 20 characteristics. This study does not use all GLCM features. Only a few features were used. For example, research [13] was using 5 magnitudes of GLCM features, namely angular second moment (ASM), contrast, inverse difference moment (IDM), entropy, and correlation.

a. Angular Second Moment (ASM)

ASM is a measurement of image homogeneity or uniformity. The ASM calculation is shown in equation (8).

$$ASM = \sum_{x=0}^{n-1}\sum_{y=0}^{n-1}\{f(x,y)\}^2 \tag{8}$$

b. Contrast

The contrast feature shows the variation of the gray level in the image matrix. Contrast calculations are shown in equation (9).

$$Contrast = \sum_{x=0}^{n-1}\sum_{y=0}^{n-1}|x-y|^2 f(x,y) \tag{9}$$

c. Inverse Difference Moment

The IDM feature is used to measure the homogeneity of images with similar degrees. The IDM calculation is shown in equation (10).

$$IDM = \sum_{x=0}^{n-1}\sum_{y=0}^{n-1}\frac{1}{1+(x-y)^2} f(x,y) \tag{10}$$

d. Entropy

$$Entropi = -\sum_{x=0}^{n-1}\sum_{y=0}^{n-1} f(x,y)log_2(f(x,y)) \tag{11}$$

e. Correlation

The correlation feature is the linear dependence of the gray level measurement of the image so that it can provide information on the existence of a linear structure in the image. Correlation calculation is shown in equation (12).

$$Correlation = \sum_{x=0}^{n-1}\sum_{y=0}^{n-1}\frac{(x\ y)f(x,y) - \mu_x\mu_y}{\sigma_x\sigma_y} \tag{12}$$

.

Where

$$\mu_x = \sum_{x=0}^{n-1} x \sum_{y=0}^{n-1} f(x,y) \tag{13}$$

$$\mu_y = \sum_{x=0}^{n-1} y \sum_{y=0}^{n-1} f(x,y) \tag{14}$$

$$\sigma_x = \sum_{x=0}^{n-1} (x-\mu_x)^2 \sum_{y=0}^{n-1} f(x,y) \tag{15}$$

$$\sigma_y = \sum_{x=0}^{n-1} (x-\mu_y)^2 \sum_{y=0}^{n-1} f(x,y) \tag{16}$$

4. Normalization of Feature Data

The feature data obtained from the feature extraction process has a wide range of values. It can adversely affect the classifier in classifying data [14]. Normalization aims to map the feature value to [0,1] by applying equation (17).

$$\text{Normalization} = \frac{data[x] - \min(data)}{\max(data) - \min(data)} \tag{17}$$

Where data [x] is the feature value in the x-index, min (data) is the smallest value in each feature data set, and max (data) is the largest value in each feature set.

**Retinal Image Classification Using Multi-Layer Perceptron (MLP)**

Multi Layer Perceptron architectures used in this study is shown in Figure 4.

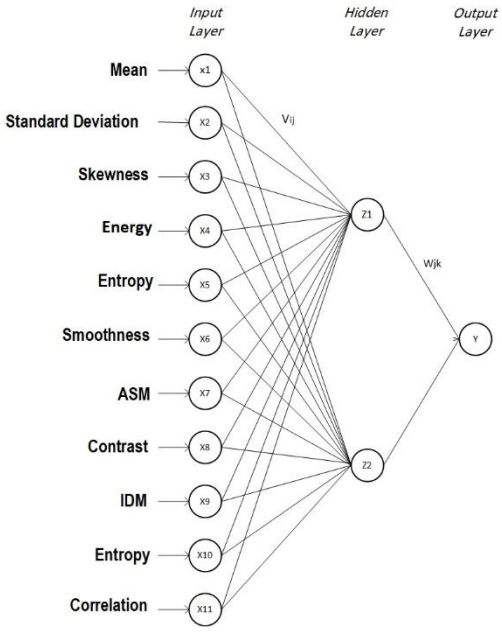


Figure 4. MLP Architectural Design

- Input Layer: The number of neurons in the input layers, there were 11 neurons. It refers to the many features used by the histogram and GLCM feature extraction methods. The data for the 11 features are presented in Table 1.

Table 1 Retinal Image Features

| No | Feature's Name | Feature Extraction Method |
|---|---|---|
| 1 | Mean | Histogram |
| 2 | Standard Deviation | |
| 3 | Skewness | |
| 4 | Entropy | |
| 5 | Energy | |
| 6 | Smoothness | |
| 7 | Angular Second Moment (ASM) | GLCM |
| 8 | Contrast | |
| 9 | Inverse Difference Moment (IDM) | |
| 10 | Entropy | |
| 11 | Correlation | |

- Hidden Layer: There is one layer with a number of neurons, namely 12 nodes.
- *Output Layer:* At the output layer, there is 1 neuron whose class labelling scheme is shown in Table 2.

Table 2 Class Labelling Schemes

| Data Class | Class Label in Binary |
|---|---|
| Normal | 0 |
| Glaucoma | 1 |

In MLP training, the backpropagation learning algorithm is used. The activation function used in this study is sigmoid. The amount of learning rate is 0.1. The number of epochs is 1000 iterations. When testing the MLP to recognize/predict retinal image data, 1 neuron is used in the output layer because there are only two data classes, namely the normal class and the glaucoma class.

## 3. RESULTS AND DISCUSSIONS

This section describes the testing results of the system that has been built. This study used two open/free datasets, namely the RIM-ONE dataset [15] and the DRISTHI-GS dataset [16]. RIM-ONE provides normal retina images with a total of 66 images used. Meanwhile, DRISTHI-GS provides 70 images of the retina affected by glaucoma, so the total data used in this study are 136 images.

The measurements of system performance used in this study are accuracy, sensitivity, and specificity. The calculations are shown in the equation 18, equation 19, and equation 20:

$$Accuracy = \frac{(TP + TN)}{(TP + FP + TN + FN)} \quad (18)$$

$$Sensitivity = \frac{TP}{(TP + FN)} \quad (19)$$

$$Specificity = \frac{TN}{(TN + FP)} \quad (20)$$

TP (True Positive) is a retinal image detected as normal, and TN (True Negative) is a retinal image detected with glaucoma. FP is a retinal image of normal retinal images predicted for glaucoma, and FN is a

retinal image of glaucoma that is predicted to be normal. Table 3 shows the test results with the 10-cross validation method against the GLCM feature extraction method, histogram, and the combined GLCM-histogram.

Table 3 MLP Test Results On A Variety Of Feature Extraction Methods

| Feature Extraction Method | Accuracy | Sensitivity | Specificity |
|---|---|---|---|
| GLCM | 68.38% | 41.79% | 94.20% |
| Histogram | 85.29% | 73.13% | 97.10% |
| GLCM-Histogram | 93.38% | 86.57% | 100% |

Based on Table 3, it can be seen that the combination of the GLCM-histogram feature extraction method obtained the accuracy, sensitivity, and specificity values in order of 93.38%, 86.57%, and 100%. Meanwhile, the GLCM method obtained an accuracy of 68.38%, 41.79% sensitivity, and 94.20% accuracy of specificity. And for feature extraction using the histogram obtained an accuracy of 85.29%, 73.13% sensitivity, and 97.10% accuracy of specificity.

## 4. CONCLUSION

This work proposed a texture-based approach for the automatic detection of glaucoma. The work used retinal fundus images in which the OD structural characteristics are segmented subsequent to texture, GLCM, and Histogram-based feature extraction. Afterward, the extracted features are classified using artificial neural networks. The combination of the GLCM and histogram feature extraction methods achieves the highest accuracy compared to employing only one of these methods. The accuracy obtained for the combined GLCM-histogram is 93.38%. Besides, the sensitivity performance is 86.57%, and the accuracy of specificity is 100%.

## REFERENCES


[1] S. Resnikoff *et al.*, "Global data on visual impairment in the year 2002," *Bull. World Health Organ.*, vol. 82, no. 11, pp. 844–851, 2004.

[2] M. Madhumalini and T. M. Devi, "Detection of Glaucoma from Fundus Images Using Novel Evolutionary-Based Deep Neural Network," *J. Digit. Imaging*, vol. 35, no. 4, pp. 1008–1022, Aug. 2022.

[3] J. Hao *et al.*, "Hybrid Variation-Aware Network for Angle-Closure Assessment in AS-OCT," *IEEE Trans. Med. Imaging*, vol. 41, no. 2, pp. 254–265, Feb. 2022.

[4] A. Manassakorn *et al.*, "GlauNet: Glaucoma Diagnosis for OCTA Imaging Using a New CNN Architecture," *IEEE Access*, vol. 10, pp. 95613–95622, 2022.

[5] P. G. Söderberg, F. Malmberg, and C. Sandberg-Melin, "Further analysis of clinical feasibility of OCT-based glaucoma diagnosis with Pigment epithelium central limit- Inner limit of the retina Minimal Distance (PIMD)," 2017, p. 100450R.

[6] M. Juneja, J. S. Minhas, N. Singla, S. Thakur, N. Thakur, and P. Jindal, "Fused framework for glaucoma diagnosis using Optical Coherence Tomography (OCT) images," *Expert Syst. Appl.*, vol. 201, p. 117202, Sep. 2022.

[7] Y. M. Chan *et al.*, "Automated detection of glaucoma using elongated quinary patterns technique with optical coherence tomography angiogram images," *Biomed. Signal Process. Control*, vol. 69, no. June, 2021.

[8] T. Khalil, M. U. Akram, S. Khalid, and A. Jameel, "An overview of automated glaucoma detection," in *2017 Computing Conference*, 2017, pp. 620–632.

[9] E. T. Gormus *et al.*, "Exploiting texture information in diagnosing Glaucoma," in *2017 25th Signal Processing and Communications Applications Conference (SIU)*, 2017, pp. 1–4.

[10] P. Sharma *et al.*, "A lightweight deep learning model for automatic segmentation and analysis of ophthalmic images," *Sci. Rep.*, vol. 12, no. 1, p. 8508, Dec. 2022.

[11] C. Bowd *et al.*, "Deep Learning Image Analysis of Optical Coherence Tomography Angiography Measured Vessel Density Improves Classification of Healthy and Glaucoma Eyes," *Am. J. Ophthalmol.*, vol. 236, pp. 298–308, 2022.

[12] N. A. Kako and A. M. Abdulazeez, "Peripapillary Atrophy Segmentation and Classification Methodologies for Glaucoma Image Detection: A Review," *Curr. Med. Imaging Former. Curr. Med. Imaging Rev.*, vol. 18, no. 11, pp. 1140–1159, Nov. 2022.

[13] C.-W. Wu, H.-Y. Chen, J.-Y. Chen, and C.-H. Lee, "Glaucoma Detection Using Support Vector Machine Method Based on Spectralis OCT," *Diagnostics*, vol. 12, no. 2, p. 391, Feb. 2022.

[14] A. P. Sunija, V. P. Gopi, and A. K. Krishna, "D-DAGNet: AN IMPROVED HYBRID DEEP NETWORK FOR AUTOMATED CLASSIFICATION OF GLAUCOMA FROM OCT IMAGES," *Biomed. Eng. Appl. Basis Commun.*, Sep. 2022.

[15] P. Jeihouni, O. Dehzangi, A. Amireskandari, A. Rezai, and N. M. Nasrabadi, "MultiSDGAN: Translation of OCT Images to Superresolved Segmentation Labels Using Multi-Discriminators in Multi-Stages," *IEEE J. Biomed. Heal. Informatics*, vol. 26, no. 4, pp. 1614–1627, 2022.

[16] E. Golkar, H. Rabbani, and A. Dehghani, "Hybrid registration of retinal fluorescein angiography and optical coherence tomography images of patients with diabetic retinopathy," *Biomed. Opt. Express*, vol. 12, no. 3, p. 1707, Mar. 2021.

[17] B. Zhou, F. Mohammadi, J. S. Lim, N. Forouzesh, H. Ghasemzadeh, and N. Amini, "Analysis of Macular Thickness Deviation Maps for Diagnosis of Glaucoma," 2021, pp. 53–64.

[18] E. Karvonen *et al.*, "Diagnostic performance of modern imaging instruments in glaucoma screening," *Br. J. Ophthalmol.*, vol. 104, no. 10, pp. 1399–1405, Oct. 2020.

[19] A. Joshi *et al.*, "Glaucoma Screening Through Level Set for Optic Disc Segmentation and Textural Features for Classification," in *2018 International Conference on Intelligent and Advanced System (ICIAS)*, 2018, pp. 1–6.

[20] A. De Gainza *et al.*, "A Metascore of Multiple Imaging Methods to Measure Long-Term Glaucoma Structural Progression," *Transl. Vis. Sci. Technol.*, vol. 11, no. 9, p. 15, Sep. 2022.

[21] N. Pankova *et al.*, "Evolving Patterns of Hyperfluorescent Fundus Autofluorescence Accompany Retinal Atrophy in the Rat and Mimic Atrophic Age-Related Macular Degeneration," *Transl. Vis. Sci. Technol.*, vol. 11, no. 3, p. 3, Mar. 2022.
[22] E. N. Iomdina, D. D. Khoziev, and P. V. Luzhnov, "Quantitative assessment of retinal and choroidal blood vessels volume using a voxel processing of optical coherence tomography angiography images," *Opt. Eng.*, vol. 60, no. 08, Mar. 2021.
[23] Y. Ma *et al.*, "ROSE: A Retinal OCT-Angiography Vessel Segmentation Dataset and New Model," *IEEE Trans. Med. Imaging*, vol. 40, no. 3, pp. 928–939, Mar. 2021.
[24] L. J. Bradley *et al.*, "Quantitative Assessment of Experimental Ocular Inflammatory Disease," *Front. Immunol.*, vol. 12, no. June, pp. 1–12, Jun. 2021.
[25] A. Septiarini and A. Harjoko, "Automatic glaucoma detection based on the type of features used: A review," *J. Theor. Appl. Inf. Technol.*, vol. 72, no. 3, pp. 366–375, 2015.
[26] M. F. Cordeiro, D. Hill, R. Patel, P. Corazza, J. Maddison, and S. Younis, "Detecting retinal cell stress and apoptosis with DARC: Progression from lab to clinic," *Prog. Retin. Eye Res.*, vol. 86, p. 100976, Jan. 2022.
[27] S. S. R. Abidi, P. C. Roy, M. S. Shah, J. Yu, and S. Yan, "A Data Mining Framework for Glaucoma Decision Support Based on Optic Nerve Image Analysis Using Machine Learning Methods," *J. Healthc. Informatics Res.*, vol. 2, no. 4, pp. 370–401, Dec. 2018.
[28] H. Masumoto, H. Tabuchi, S. Nakakura, N. Ishitobi, M. Miki, and H. Enno, "Deep-learning Classifier With an Ultrawide-field Scanning Laser Ophthalmoscope Detects Glaucoma Visual Field Severity," *J. Glaucoma*, vol. 27, no. 7, pp. 647–652, Jul. 2018.
[29] W. Gong, X. Lu, and G. Wang, "Asymmetry of Optic Nerve Head Parameters Measured by Confocal Scanning Laser Ophthalmoscopy in Myopic Anisometropic Eyes," *Appl. Sci.*, vol. 12, no. 8, p. 4047, Apr. 2022.
[30] N. Nicolini *et al.*, "Assessment of Diabetic Choroidopathy Using Ultra-Widefield Optical Coherence Tomography," *Transl. Vis. Sci. Technol.*, vol. 11, no. 3, p. 35, Mar. 2022.
[31] T. Soomro, N. Shah, M. Niestrata-Ortiz, T. Yap, E. M. Normando, and M. F. Cordeiro, "Recent advances in imaging technologies for assessment of retinal diseases," *Expert Rev. Med. Devices*, vol. 17, no. 10, pp. 1095–1108, Oct. 2020.
[32] C. Liu and L. Wang, "Functional photoacoustic microscopy of hemodynamics: a review," *Biomed. Eng. Lett.*, vol. 12, no. 2, pp. 97–124, May 2022.
[33] S. Das *et al.*, "Feasibility and clinical utility of handheld fundus cameras for retinal imaging," *Eye*, no. June 2021, pp. 1–6, Jan. 2022.
[34] L. Pascal, O. J. Perdomo, X. Bost, B. Huet, S. Otálora, and M. A. Zuluaga, "Multi-task deep learning for glaucoma detection from color fundus images," *Sci. Rep.*, vol. 12, no. 1, pp. 6–15, 2022.
[35] Y. Hagiwara *et al.*, "Computer-aided diagnosis of glaucoma using fundus images: A review," *Comput. Methods Programs Biomed.*, vol. 165, pp. 1–12, 2018.
[36] N. Varma, S. Yadav, and J. K. P. S. Yadav, "A Short Review on Automatic Detection of Glaucoma Using Fundus Image," 2023, pp. 493–504.
[37] L. K. Singh, M. Khanna, and S. Thawkar, "A novel hybrid robust architecture for automatic screening of glaucoma using fundus photos, built on feature selection and machine learning-nature driven computing," *Expert Syst.*, vol. 39, no. 10, Dec. 2022.
[38] A. Qayyum, W. Sultani, F. Shamshad, R. Tufail, and J. Qadir, "Single-shot retinal image enhancement using untrained and pretrained neural networks priors integrated with analytical image priors," *Comput. Biol. Med.*, vol. 148, p. 105879, Sep. 2022.
[39] M. Arhami, A. Desiani, S. Yahdin, A. I. Putri, R. Primartha, and H. Husaini, "Contrast enhancement for improved blood vessels retinal segmentation using top-hat transformation and otsu thresholding," *Int. J. Adv. Intell. Informatics*, vol. 8, no. 2, p. 210, Jul. 2022.
[40] V. V. Starovoitov, Y. I. Golub, and M. M. Lukashevich, "A Universal Retinal Image Template for Automated Screening of Diabetic Retinopathy," *Pattern Recognit. Image Anal.*, vol. 32, no. 2, pp. 322–331, Jun. 2022.
[41] A. Septiarini, A. Harjoko, R. Pulungan, and R. Ekantini, "Optic disc and cup segmentation by automatic thresholding with morphological operation for glaucoma evaluation," *Signal, Image Video Process.*, vol. 11, no. 5, pp. 945–952, Jul. 2017.
[42] F. Guo, W. Li, J. Tang, B. Zou, and Z. Fan, "Automated glaucoma screening method based on image segmentation and feature extraction," *Med. Biol. Eng. Comput.*, vol. 58, no. 10, pp. 2567–2586, Oct. 2020.
[43] S. Karthikeyan and N. Rengarajan, "Performance analysis of gray level cooccurrence matrix texture features for glaucoma diagnosis," *Am. J. Appl. Sci.*, vol. 11, no. 2, pp. 248–257, 2013.
[44] U. R. Acharya, S. Dua, X. Du, V. Sree S, and C. K. Chua, "Automated Diagnosis of Glaucoma Using Texture and Higher Order Spectra Features," *IEEE Trans. Inf. Technol. Biomed.*, vol. 15, no. 3, pp. 449–455, May 2011.
[45] R. Touahri, N. Azizi, N. E. Hammami, M. Aldwairi, N. E. Benzebouchi, and O. Moumene, "Multi source retinal fundus image classification using convolution neural networks fusion and Gabor-based texture representation," *Int. J. Comput. Vis. Robot.*, vol. 11, no. 4, p. 401, 2021.
[46] D. Yadav, M. P. Sarathi, and M. K. Dutta, "Classification of glaucoma based on texture features using neural networks," *2014 7th Int. Conf. Contemp. Comput. IC3 2014*, pp. 109–112, 2014.
[47] K. Sonti and D. R. Dhuli, "Shape and texture based identification of glaucoma from retinal fundus images," *Biomed. Signal Process. Control*, vol. 73, no. December 2021, p. 103473, 2022.

.